Electrochemistry of Metal Nanoparticles and Quantum Dots

27

Antonio Doménech-Carbó, Raquel E. Galian, Jordi Aguilera-Sigalat, and Julia Pérez-Prieto

Contents

Abstract

Metal nanoparticles, with a wide range of applications in catalysis and sensing, have structural and electronic properties that differ from those of their bulk macroscopic counterparts. Electrochemical techniques are of particular interest in the study of metal nanoparticles because electrons may undergo quantum confinement effects which are reflected in their electrochemical behavior, resulting, ultimately, in three distinguishable voltammetric regimes: bulk continuum, quantized double-layer charging, and molecule-like. Similarly, semiconductor nanoparticles (quantum dots, QDs) are receiving considerable

A. Doménech-Carbó (✉)
Departamento de Química Analítica, Universidad de Valencia, Burjassot, Valencia, Spain
e-mail: antonio.domenech@uv.es

R.E. Galian • J. Aguilera-Sigalat • J. Pérez-Prieto
Instituto de Ciencia Molecular (ICMol), Universidad de Valencia, Paterna, Valencia, Spain

M. Aliofkhazraei (ed.), *Handbook of Nanoparticles*,
DOI 10.1007/978-3-319-15338-4_28

attention due to their high fluorescence, which makes them of interest for biological and medical applications, among others. The semiconductor bulk materials possess defect states that originate from impurities, divacancies, or surface reactions as a result of their synthesis. Voltammetric features provide information on bandgap energy, the position of conduction and valence band edges, and the position of defect sites as well as on the interaction with the capping ligand. This chapter is devoted to provide a critical view of the current state of the art in the electrochemistry of such systems.

Keywords
Electrochemical techniques • Metal nanoparticles • Quantum dots • Electrocatalysis

Introduction

Metal and semiconductor nanoparticles, nanowires, nanopores, and other systems of dimensions at the nanometric scale have structural and electronic properties that differ from those of their bulk macroscopic counterparts. The study of the electrochemistry of such systems, i.e., that of the processes involving interfacial charge transfer between nanosized systems and electron-conducting electrodes, possesses a great importance by either its ability to yield relevant information on the structure and composition of nanoparticulate entities and their applications in catalysis and sensing [1, 2]. Here, the attention will be focused on nanoparticulate systems constituted by a core of metal atoms, surrounded or not by a coating of metal compounds, and stabilized by a monolayer (capping) of organic ligands that prevent agglomeration. The electrochemistry of nanoparticulate films, nanoelectrodes, and nanopores will be treated only tangentially.

In principle, the term nanoparticle electrochemistry refers to that of metal and semiconductor colloids, also termed colloidal microelectrodes [3, 4], differing from conventional colloids by their ability to act as electron donors and acceptors [5, 6]. Typically, the electrochemistry of solutions of metal nanoparticles and quantum dots in electrolytes is studied by means of voltammetric methods. Several general aspects should be underlined [7, 8]:

(a) The voltammetric response of the nanoparticulate systems can be superimposed to that of electroactive ligands.
(b) Measurements can be performed both on nanoparticulate solutions (or dispersions) and on thin films of nanoparticles deposited on the electrode surface.
(c) In contrast with, for instance, spectroscopic techniques which provide information on the "bulk" nanoparticle composition, electrochemical methods mainly probe the surface properties of those systems [9, 10].
(d) There is a number of applications for sensing, photoelectrochemical functional devices, electrosynthesis, anticorrosion, and environmental remediation,

Table 1 Earlier insights into the development of nanoparticles electrochemistry

Matter	Citation(s)
Electron donor/acceptor properties of metal and semiconductor colloids	Henglein [5]; Kiwi and Grätzel [6]
Metal nanoparticles and water splitting	Miller et al. [11]
Stabilizing nanoparticles by means of organic ligands	Schmid et al. [12]
Role of metal and semiconductor colloids as redox mediators	Henglein [4]
Quantum dots	Bawendi et al. [13]
Modeling molecular capacitance	Weaver and Gao [14]
Chemical linking of metal nanoparticles to electrodes	Chumanov et al. [15]; Grabar et al. [16]
Bulk-continuum voltammetry of metal nanoparticles	Ung et al. [17]
Quantized double-layer charging of metal nanoparticles	Ingram et al. [18]
Quantum confinement effects	Chen et al. [19]
Electrodeposition of metal nanoparticles	Finot et al. [20]

involving nanoparticulate systems with different nanoarchitectures and/or involving different types of functionalization and/or forming a variety of nanocomposites.

The earlier historical development of nanoparticle electrochemistry can be summarized in a series of insights, some of which are listed chronologically in Table 1.

Nanoparticles electrochemistry can be viewed as a new field located at an intermediate-size scale between molecular electrochemistry and solid state electrochemistry [21]. Figure 1 shows a schematic view of the position of nanoparticle electrochemistry and its previously mentioned aspects.

Electrochemical Techniques

Conventional electrochemical techniques have been used in the chemistry of nanomaterials to characterize the nanomaterial surface. Electrochemical techniques are particularly interesting by their capability of yielding information by using standard instrumentation. Regarding to the sample experimental condition, the electrochemical measurements can be done in a colloidal solution or in a film. In the first case, the in general low solubility of the nanoparticles in the media reduces the electrochemical signal and the sensibility of the system. The deposition of the nanoparticles on the electrodes has been used to overcome this problem [7]. In general, electrochemical techniques are used for analytical purposes, but they can also be used for preparative ones, for instance, for electrodeposition of nanoparticles on substrates [22] and liquid–liquid interfaces [23].

The most used electrochemical techniques can be divided into static and dynamic, depending on the type of electrochemical processes occurring at the

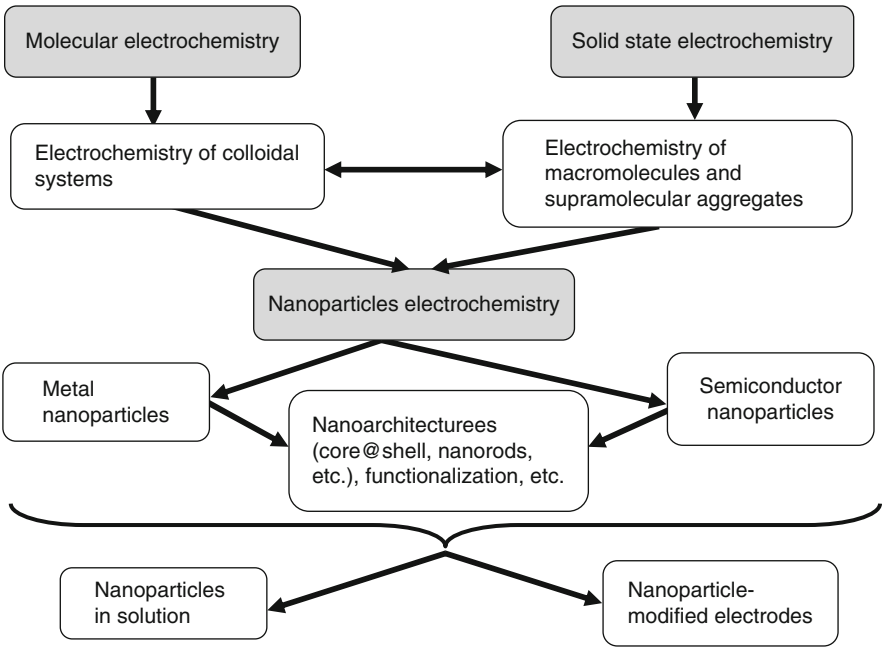

Fig. 1 Scheme of possible relationships among topics typically involved in nanoparticles electrochemistry

electrode/electrolyte interface. As summarized in Fig. 2, the main static methods are potentiometry, electrochemical noise, and impedance measurements (electrochemical impedance spectroscopy in particular). Dynamic methods involve faradaic processes recorded by means of coulometry, chronoamperometry, chronopotentiometry and, particularly, voltammetry. Chronoamperometric and chronocoulometric techniques can be used conjointly with voltammetric ones, whereas electrochemical impedance spectroscopy is of application in the analysis of microparticulate films. Several static and dynamic techniques can be hyphenated with optical (X-ray diffraction, spectroelectrochemistry) and microscopy imaging techniques such as atomic force microscopy (AFM). In the particular case of semiconductor quantum dots, the most used electrochemical techniques can be grouped into voltammetric (cyclic, differential pulse, square wave voltammetry), electrochemiluminescence, and spectroelectrochemistry [8]. Electrochemical imaging techniques are increasingly used to study nanoparticle films on electrodes. The scanning electrochemical microscopy technique (SECM), developed by Bard et al. [24], uses a tip microelectrode as a local probe providing spatially resolved information on the redox reactivity of surfaces and has been used for measurement on electron transfer dynamics [25] and local deposition of nanoparticles [22, 26]. Recent developments involve the use of optical signals of the electrode, namely, surface plasmon resonance [27], and combination with AFM in order to probe individual metal nanoparticles [28].

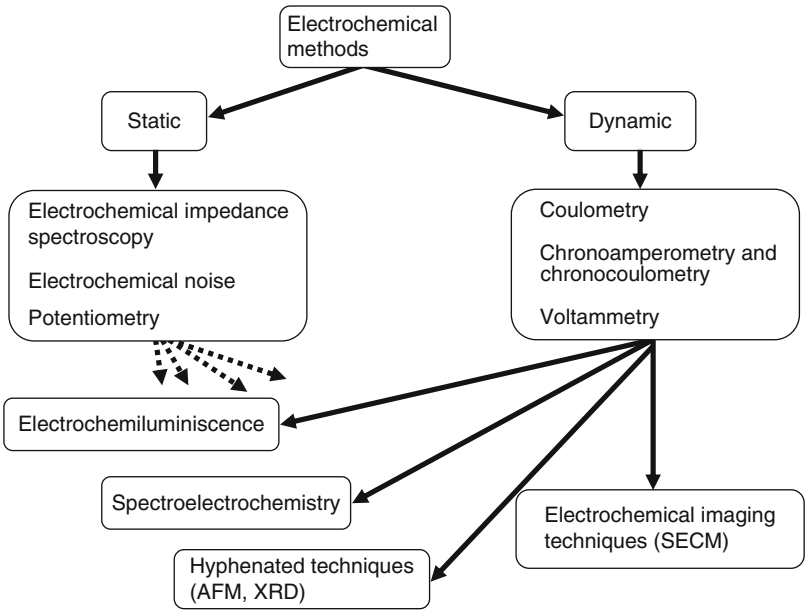

Fig. 2 Scheme illustrating the main electrochemical techniques used in nanoparticle electrochemistry

Spectroelectrochemistry techniques combine spectroscopic and electrochemical methods, thus facilitating the interpretation of electron transfer reactions. For example, they can give valuable information in photoinduced electron transfer processes by providing static-state products analogous to those that are generated in transient spectroscopy. Among the spectroscopic techniques, the steady-state and time-resolved optical ones are having a special relevance in nanoparticle spectroelectrochemistry. For these measurements, the electrochemical cell, housing a working, a reference, and a counter electrode, is designed to be simultaneously used for electrochemistry and spectroscopy, and consequently, the spectra are recorded while the potential is stepped to a desired value. Thus, the design of the cell for electrochemiluminescence is such that it can be inserted into the sample compartment of an emission spectrophotometer.

Electrochemical Behaviors

Quantum Confinement Effects

In a solid metal or semiconductor material, electronic energy levels are distributed forming quasi-continuum bands. When the size of the particle is reduced to few nanometers, quantum confinement effects appear and the band structure of the semiconductor changes into discrete levels. As a result, the optical and electrical

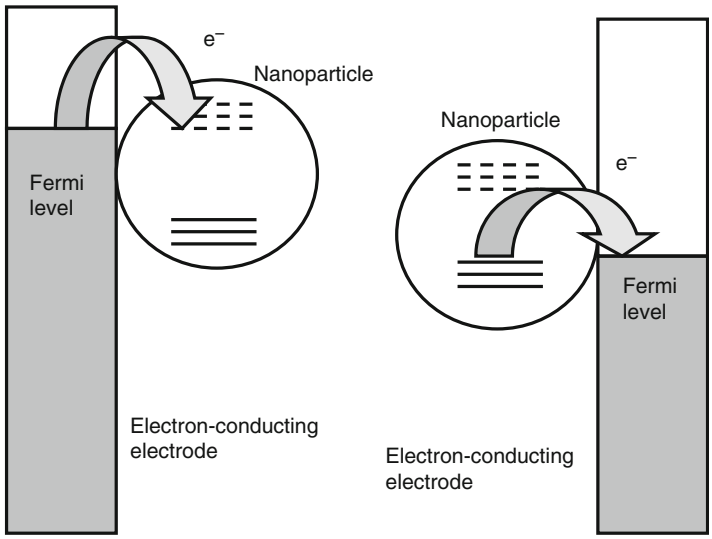

Fig. 3 Schematic representation of electrochemical processes involving nanoparticles. *Left*: injection of an electron from the Fermi level of the metal electrode to the conduction band of the particle; *right*: electron extraction from the nanoparticle to the Fermi level of a metal electrode (equivalent to the injection of a hole into the valence band of the nanoparticle)

properties become dependent on its physical dimension; in particular, the electrochemical response becomes size dependent. For our purposes it is pertinent to remark that electronic levels separate into conduction and valence bands and the energy difference between the highest occupied molecular orbital (HOMO) and the lowest unoccupied molecular orbital (LUMO) widens as the particle size decreases [29–31]. This yields an energy gap which can be optically and/or electrochemically detected (*vide infra*). Then, the nanoparticulate system behaves similarly to semiconductor electrochemistry. Figure 3 shows a schematic representation of the basic electron transfer processes between an electron-conducting electrode and a nanoparticle having a band gap. Electrochemical reduction processes can be described as the injection of an electron from the Fermi level of the metal electrode to the conduction band of the particle. Electrochemical oxidation can be represented by an extraction of an electron from the valence levels of the particle to the Fermi level of a metal electrode. This process can be considered as similar to the injection of a hole into the valence band of the nanoparticle.

Roughly speaking, there is a continuous-like transition from the metal (or semiconductor) "bulk" state to the molecule-like behavior, so that following Murray [7], three electrochemical regimes can be differentiated by means of voltammetric methods, namely, bulk continuum, quantized double-layer charging, and molecule-like. When the organic ligand monolayer of the nanoparticles contains electroactive groups, the electrochemical response of such groups can be recorded, thus incorporating additional signals to the voltammetry response of the

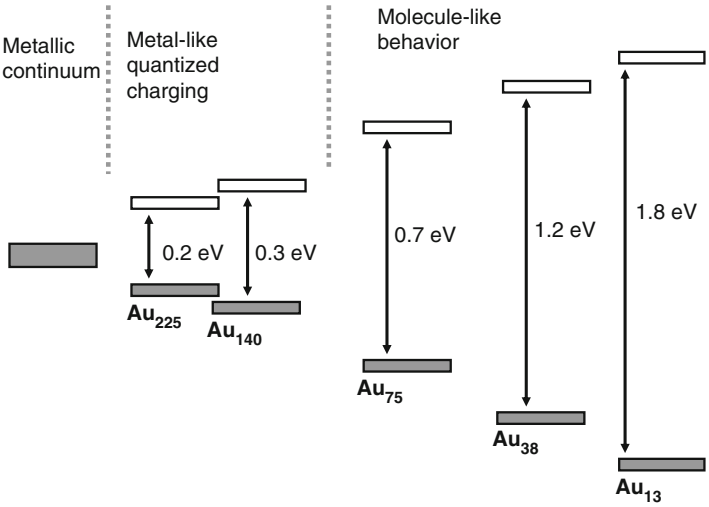

Fig. 4 Schematic representation of the variation of the electrochemical response of Au nanoparticles showing optical HOMO-LUMO energy gaps (Adapted from Ref. [7] using data from Refs. [14, 32–37])

nanoparticulate system. Figure 4 shows a schematic representation for the shift from the continuum electrochemical response to the molecule-like behavior for Au nanoparticles [7, 14, 32–36]. In the case of semiconductors, the bandgap of the bulk material can be increased by nanostructuring the material via quantum confinement effects, and the band-edge energies can be subsequently tuned by passivating the surface with dipolar ligands [37].

Bulk-Continuum Response

The bulk-continuum behavior is typical of nanoparticles having sizes larger than 3–4 nm. Such systems behave as capacitors with double-layer capacitance C_{NP}, directly related to the change in electrochemical potential (ΔV) associated to the transfer of z electrons from/to the nanoparticle to/from the electrode:

$$\Delta V = ze/C_{NP} \tag{1}$$

If ΔV is of the same order of magnitude or lower than the Boltzmann thermal energy distribution factor ($k_B T$), successive electron transfers from/to the particle will result in a continuous change in the particles potential. In these circumstances, the capacitive charging currents are under mass transport control and can be distinguished from double-layer charging and faradaic reactions at the electrode/electrolyte interface using conventional chronoamperometric, chronocoulometric, and/or rotating disk voltammetric experiments. In the case of Ag nanoparticles

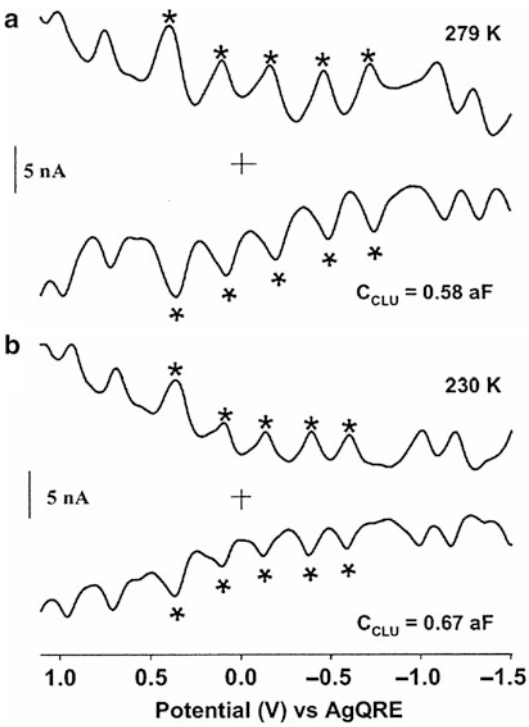

Fig. 5 Differential pulse voltammetry of 0.07 mM ethanol-soluble hexanethiolate-MPCs at (**a**) 279 and (**b**) 230 K in dichloromethane/0.05 M Bu_4NClO_4 at 1.6-mm diameter Pt working electrode, Pt coil counter electrode, and Ag wire quasireference electrode (0.05 V pulse, 50-ms pulse width, 200-ms period, 0.02 V/s scan rate) [40]. The *asterisks* mark the peaks used for determining the capacitance of the nanoparticles (Reprinted with permission from Miles and Murray [40]. Copyright (2003) American Chemical Society)

capped with polyacrylic acid, application of anodic potentials produced currents for the oxidative dissolution of nanoparticles (*vide infra*) while applying negative potentials yields featureless, progressively rising currents under mass transfer control so that for sufficiently negative potentials ca. 1,600 electrons/nanoparticle were transferred, corresponding to a capacity of 80 μF/cm^2 [37], clearly higher than those typically obtained at conventional metal electrodes under equivalent conditions.

Quantized Double-Layer Charging

This electrochemical regime is characterized by the record of multiple peak features corresponding to quantized double-layer charging. First reported by Ingram et al. [18], these features have been intensively studied, as can be seen in recent reviews [38, 39]. A typical example can be seen in Fig. 5, where differential pulse voltammograms for monolayer alkanethiolate-protected Au nanoclusters at different temperatures are shown [40]. The voltammogram consists of a series of peaks almost equally spaced, which can be attributed to quantized charge processes [41].

Such systems can be described as a concentric spherical capacitor assuming that the metal core, of radius *r*, is surrounded by a monolayer of capping (typically,

thiolate compounds) of thickness d, of effective dielectric permittivity ε. The capacity of this system is

$$C = 4\pi\varepsilon\frac{r}{d}(r+d) \tag{2}$$

Charging processes can be viewed as sequential reversible one-electron transfers on metal nanoparticles, M, represented as

$$\mathrm{M}^n + \mathrm{e}^- \rightarrow \mathrm{M}^{n-1} \tag{3}$$

where $n = 0, -1, -2$, etc. The simplest theoretical approach considers the metal nanoparticles to be a conducting sphere with the energetics of electron addition determined by classical electrostatics [14, 42, 43]. This model predicts the appearance of identical voltammetric waves corresponding to the successive transfer of electrons giving rise to successive z, $z-1$, $z-2$, etc., charge states [44, 45]. The formal electrode potential of the $z/z-1$ charge state change is given by

$$E^o_{z,z-1} = E_{\mathrm{PZC}} + \frac{(z-1/2)e}{C} \tag{4}$$

where E_{PZC} is the potential of zero charge for the nanoparticle core.

Deviations from the expected uniform potential spacing between voltammetric peaks appear at high charge states and are dependent on the solvent, on the electrolyte composition, and, in particular, on the length of the alkanethiolate chain [41]. These features can be mainly attributed to the variations in the permittivity of the capping monolayer. The peak spacing is also conditioned by the length and flexibility of the protecting (typically alkanethiolate) molecules, allowing for a more or less profound penetration of the solvent between them. Apart from the above effects, diffuse layer effects associated to the Helmholtz double-layer surrounding the nanoparticles also influence the observed peak spacing [32]. Supporting electrolyte anion-dependent effects can be interpreted as the result of different ion-pairing effects [46]. Ultimately, the incipient influence of the molecule-type response can also distort the uniform peak spacing response. Doublet oxidation peaks, a typical feature of electron transfer at molecular species, often appear, but the interpretation of such features still remains controversial [47, 48].

Molecule-Type Behavior

For sufficiently small nanoparticles, there is an energy bandgap which can be detected, but not equivalently, by means of optical and electrochemical measurements. The optical band gap, ΔE_{op}, corresponds to transitions between the highest occupied molecular orbital (HOMO) and the lowest unoccupied molecular orbital (LUMO), detectable as absorption band edges in the visible or near-infrared region. The electrochemical energy gap, ΔE_{el}, is the difference between the

electrochemical potentials for the first oxidation and first reduction wave for a parent species. The electrochemical bandgap is in general in good agreement with the difference between them, increasing the importance of the quantum confinement effects (i.e., for small particles), resulting in an increased Coulombic electron–hole interaction term (i.e., the energy associated to the generation of separated charges), $J_{e,h}$. Then,

$$\Delta E_{op} = \Delta E_{el} - J_{e,h} \tag{5}$$

The value of $J_{e,h}$ for the smaller particles can be calculated as ca. 0.1 eV. This term does not apply for optical HOMO–LUMO transitions, where no change in the overall charge of the nanoparticle occurs.

In the case of alkanethiol-capped metal nanoparticles, appearance of a HOMO–LUMO energy gap is reflected by an enlarged potential spacing between the current peaks for the first one-electron loss and the first one-electron gain of the parent nanoparticle (Fig. 6) [50]. The molecule-like behavior appears to be dependent on the electronic interactions between the particle core and capping ligands. Thus, electron-donating cappings such as phosphines would lead to an increase of the particle core electron density and hence a negative (upward) shift of the Fermi level. Opposite behavior is expected from electron-acceptor cappings, typically thiol-protecting ligands, resulting in a decrease of the electron density of the Au core [49].

It is pertinent to note that uncertainty remains about the so-called formulaic composition of the nanoparticulate system, expressed in terms of $[metal]_x[stabilizing\ ligands]_{y,z}$ [7], so that, in general, nanoparticulate systems are designed by their diameter, which is typically estimated from TEM images and spectral data.

An interesting, directly related case is that of metal nanoparticles covered by a metal oxide shell. Voltammetric experiments suggest that oxidation of Pd@PdO nanoparticle in aqueous alkaline electrolyte could proceed via formation of Pd $(OH)_x$ adsorbed species further evolving to Pd oxides and/or Pd^{2+} ions in solution [51], similarly to the growth of porous PdO films on Pd electrodes [52]. Solid state electrochemistry of nanoheterogeneous deposits of Pd nanoparticles covered by PdO shell on graphite electrodes in contact with aqueous permits a direct estimation of the thickness of the PdO shell and the size of the palladium core by using electrochemical data alone [51].

In the case of CdSe and CdTe quantum dots, nanocrystals are usually endowed with surface monolayers composed of ligands such as trioctylphosphine oxide (TOPO), *n*-decanethiol, and TOPO/*n*-hexadecylamine. Cyclic voltammetric experiments on QD dispersions [52] and adsorbed on electrode surfaces [53] have been used for determining energy band gaps, the relationship between optical and electrochemical band gaps being expressed by Eq. 5. It has been reported that the electrochemical bandgap energy of *n*-decanethiol-coated samples decreases on increasing the core diameter of the QD, the electrochemical bandgap being consistently 0.4–0.5 eV smaller than the optical bandgap [8]. This discrepancy, which is

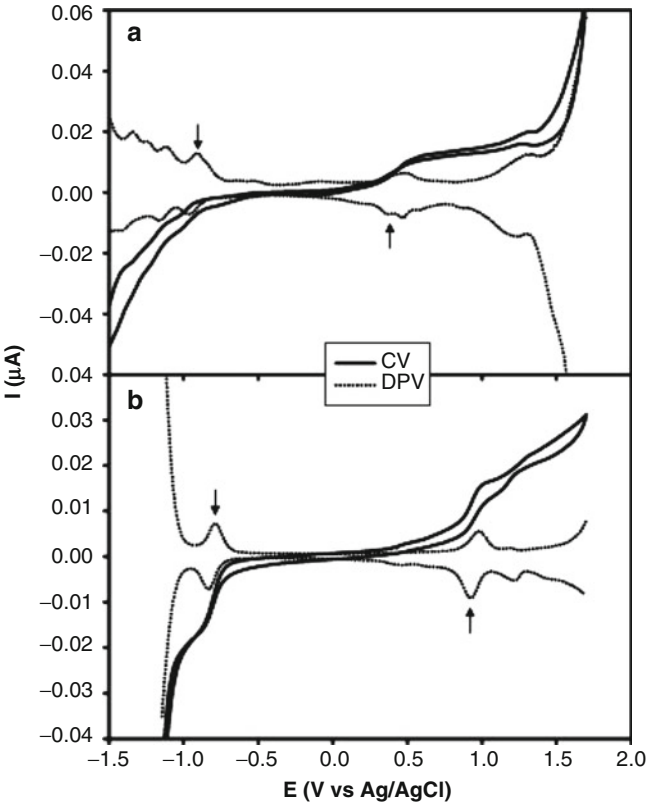

Fig. 6 Cyclic (CVs) and differential pulse voltammograms (DPVs) of $Au_{11}Cl_3(PPh_3)_7$ nanoparticles before (**a**) and after (**b**) exchange reactions with *n*-dodecanethiols at a Pt microelectrode (25 μm). The particle solutions were prepared in CH_2Cl_2 with 0.1 M TBAP at a concentration of 0.5 mM (**a**) and 1.2 mM (**b**), respectively. CV potential scan rate 20 mV/s; in DPV measurements, dc potential ramp 20 mV/s, pulse amplitude 50 mV. *Arrows* indicate the first positive and negative voltammetric peaks [49] (Reprinted with permission from Yang and Chen [49]. Copyright (2003) American Chemical Society)

clearly larger than that estimated for the Coulombic interaction energy, has been attributed to the presence of surface defects that act as local trap states for electrons and holes [8, 54]. The presence of additional peaks in the voltammograms of quantum dots has been attributed to inter-band trap states. This assignment is consistent with the presence of a broad band on the low-energy side of the band-edge photoluminescence or the appearance of a new band at longer wavelengths [55].

In the case of CdSe/ZnS QDs, electrochemical data suggest that the ZnS shell does not affect the charge injection to the CdSe core. This has been attributed to the occurrence of electron injection at potentials below those corresponding to the conduction energy level for ZnS [56]. Replacing usual capping ligands by

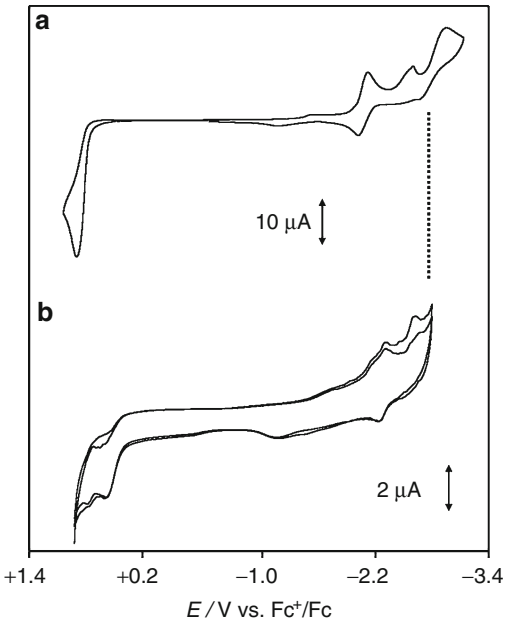

Fig. 7 Cyclic voltammograms at glassy carbon electrode of (**a**) 1 mM *N*-(2-mercaptoethyl)-1,8-naphthalimide, (**b**) 6 μM CdSe/ZnS QDs capped with that ligand in 0.10 M Bu_4NPF_6 solution in 1/1 toluene/MeCN (v/v). Potential scan rate 50 mV/s. The *dotted line* separates the region of largely negative potentials where electrolyte signals appear (Reprinted with permission from Aguilera-Sigalat et al. [58]. Copyright (2013) American Chemical Society)

electroactive ones results in shifts in the peak potentials for QD oxidation and reduction, but also in the modification of the electrochemical response of the ligand [57].

It is pertinent to note that in general it is difficult to discern between the genuine signals of the nanoparticle system and those due to the "free" electroactive cappings (such as thiolate species) and even those due to the supporting electrolyte/solvent system. An example can be seen in Fig. 7, where cyclic voltammograms at glassy carbon electrode of *N*-(2-mercaptoethyl)-1,8-naphthalimide and of CdSe/ZnS nanoparticles capped with this ligand in 1/1 toluene/acetonitrile (v/v) solution [58]. The ligand displays an irreversible, thiol-localized oxidation at largely positive potentials and an essentially reversible couple at ca. −1.8 V vs. Fc^+/Fc, ascribed to the reduction of the carbonyl unit. This couple is considerably diminished in the naphthalimide-capped QD and is accompanied by a series of additional voltammetric features which can be assigned to the QD signals, formally represented in terms of the CdSe/Se° (oxidation) and CdSe/Cd° (reduction) couples.

Figure 8 permits to observe intermediate signals accompanying extreme QD signals defining the electrochemical band gap. Such signals have been interpreted in terms of charge transfer processes involving defect states of the QDs. Intermediate oxidation processes would correspond to capping-mediated electron release from defect sites of the QDs, whereas intermediate reduction would correspond to the electron transfer to empty energy levels of the QD. Interestingly, the separation of the intermediate QD-localized voltammetric peaks relative to the extreme QD peaks appears to be coincident with the position of the different trap energy levels

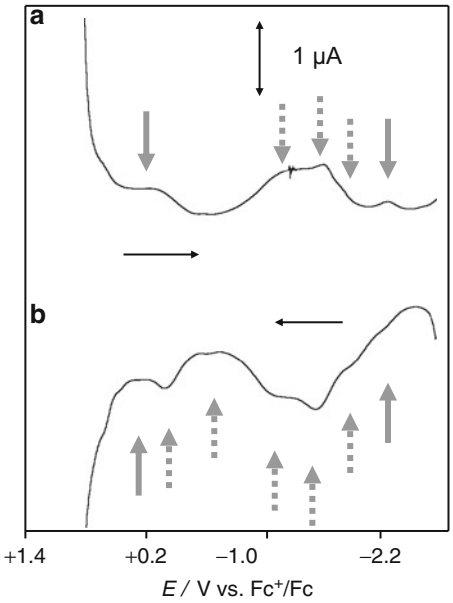

Fig. 8 Square-wave voltammograms at glassy carbon electrode of 6 μM solution of CdSe/ZnS QDs capped with long chain primary amine in 1/1 (v/v) toluene/MeCN (0.10 M Bu_4NPF_6). Potential scan initiated at (**a**) +0.80 V in the negative direction and (**b**) −2.7 V in the positive direction. Potential step increment 4 mV; square wave amplitude 25 mV; frequency 5 Hz. Extreme QD signals are marked by *solid arrows* while intermediate QD-localized ones are marked by *dotted arrows* [58] (Reprinted with permission from Aguilera-Sigalat et al. [58]. Copyright (2013) American Chemical Society)

for the different types of defect sites reported in the literature [59]. However, the relative intensity of the intermediate peaks is clearly capping dependent, so that the role of the ligand would be, to some extent, the "activation" of the trap states [58].

Electrochemical Characterization of Nanoparticles

The oxidative dissolution of metal nanoparticles is also a size-dependent process, so that the standard electrode potential for the oxidation of, for instance, Ag nanoparticles, $E^{o}_{M,NP}$, differs from that for the oxidation of the bulk metal, $E_{M,bulk}{}^{o}$, by one term including the surface tension, σ; the molar volume, v_M; the lowest valence state, z; and the nanoparticle radius, r [60, 61]:

$$E^{o}_{M,NP} = E^{o}_{M,bulk} - 2zv_M/zFr \tag{6}$$

Recently, Brainina et al. have proposed a size-dependent model for the oxidative dissolution of metal nanoparticles based on the above considerations, showing an excellent agreement with experimental data [62–65]. Here, the peak profile for

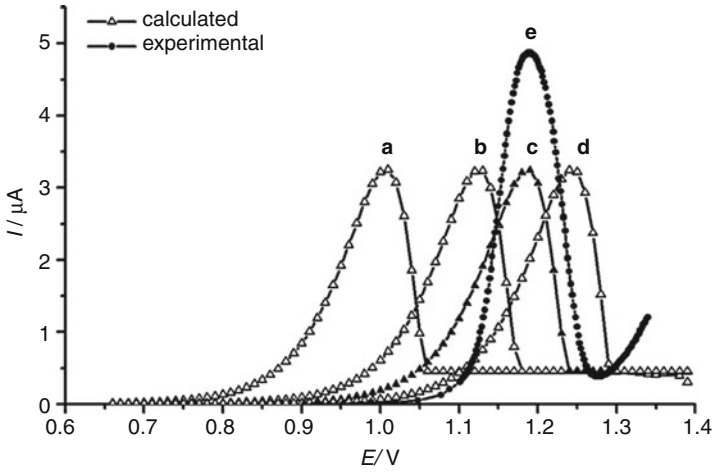

Fig. 9 Experimental (*circle*) and calculated (*triangular*) voltammograms of the gold particles electrooxidation in 0.1 M HCl; potential scan rate 50 mV/s. Calculation parameters: $Q = 10.07$ μC, $\delta = 1$ (*a*); $Q = 11.30$ μC, $\delta = 1$ (*c*); $Q = 14.57$ μC, $\delta = 1$ (*b*); $Q = 49.42$ μC, $\delta = 0.3$ (*d*) [65] (Reprinted with permission from Brainina et al. [65]. Copyright (2012) Springer)

metal nanoparticle oxidation is made dependent on the fraction of particles of a certain size, δ, and the surface tension of gold on the boundary with air. An excellent agreement was obtained between theory and experiment, as shown in Fig. 9.

It should be noted that, in general, electrochemical oxidation of metal nanoparticles can lead not only to metal ions in solution but also to the formation of metal oxides via, in the case of Pt, the following processes:

$$\mathrm{Pt} \rightarrow \mathrm{Pt}^{2+}(\mathrm{aq}) + 2\mathrm{e}^- \tag{7}$$

$$\mathrm{Pt} + \mathrm{H_2O} \rightarrow \mathrm{PtO(s)} + 2\mathrm{H}^+(\mathrm{aq}) + 2\mathrm{e}^- \tag{8}$$

The electrochemical stability under "thermodynamic" conditions would be size dependent, so that particle size-dependent potential vs. pH diagrams such as in Fig. 10 can be constructed [67].

Compton et al. have provided theoretical modeling of charge diffusion on the surface of immobilized spherical particles [67], voltammetry at random microparticle arrays [68], and dissolution of microparticle arrays [69] and nanoparticle detection [70]. Direct oxidation of the Ag nanoparticles during collision events was monitored by the presence of a spike under oxidative current. The onset potential of the spike changes with the potential and can be used to determine the size of the nanoparticle. This method can be used to identify Ag NPs (onset spike potential vs. anodic stripping voltammetry of the NPs) and to analyze their size by taking into account the charge passed per current spike [70]. Surface agglomeration of Ag nanoparticle has been recently described using the anodic stripping voltammetry.

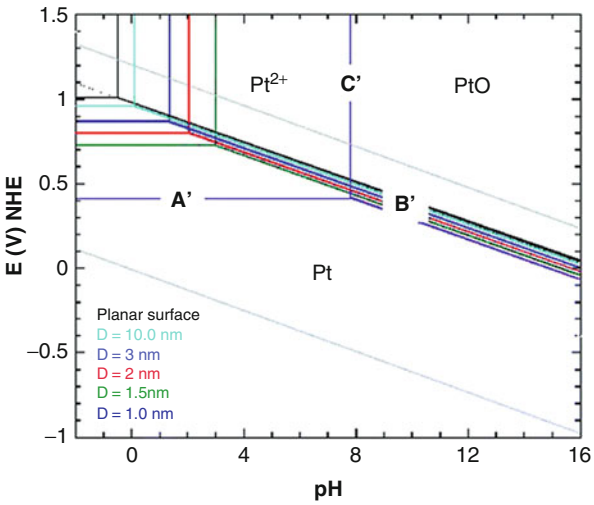

Fig. 10 Particle-size-dependent potential-pH diagram for Pt/10^{-6} M, Pt^{2+} [66] (Reprinted with permission from Tang et al. [66]. Copyright (2010) American Chemical Society)

New analytical expressions were reported for the stripping voltammetry, and they demonstrate that the oxidation peak potential for the stripping of the metallic nanoparticle should be below the formal potential for the oxidation. Changes in the response of the stripping peak potential as a function of the surface coverage give information about the nanoparticle distribution and can be related to the surface agglomeration of the NPs [71]. Electrodeposition of monolayers [72] or multilayers [73] of a second metal on a metal nanoparticle has also been reported.

Bard et al. [74] have proposed a new and simple methodology for the study of the nanoparticles at the single particle level (single-molecule electrochemistry). It is well known that only few electrons can be transferred between the nanoparticle and the electrode, and consequently, a small current can be determined, resulting in a small signal that can be confused with the background noise. The proposed methodology is based on the large current amplification ("staircase") generated in an electroactive redox probe whose oxidation or reduction is catalytically enhanced at nanoparticulate films on electrodes. This methodology has been applied to the reduction of proton and hydrogen peroxide at very low concentrations as well as to the oxidation of hydrazine occurring in Pt nanoparticle solutions. The electrocatalytic effect occurs (see scheme in Fig. 11) when the nanoparticles collide with the inert electrode [75]. These single nanoparticle collisions are characterized as current transients (electrocatalytic amplification) and are used to estimate the nanoparticle size. Single IrO_x nanoparticles can also be detected on the basis of the increase of the signal ("spike") produced when the IrO_x nanoparticle and the Pt electrode are in contact for the hydrogen production, which does not occur in absence of the nanoparticle [76]. Stochastic electrochemistry with metal and metal oxide nanoparticles at inert electrodes has been modeled in terms of NP collisions, differing from the usual model for ensemble-based electrochemical behavior [77].

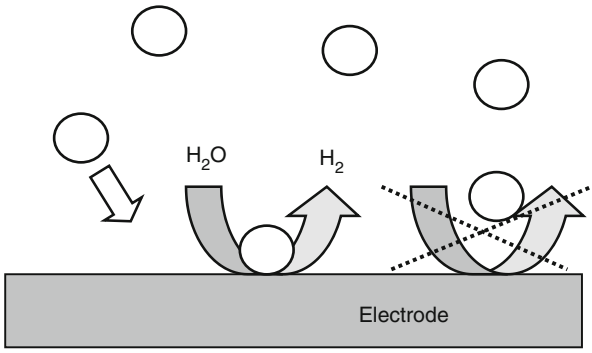

Fig. 11 Electrochemical water oxidation in the nanoparticle surface occurs when the nanoparticles are in contact with an electrode

The role of counterions into the electrochemical response of gold nanoparticles on a monolayer films has been reported. Electrochemical charging was observed with small counterions like BF_4^-, ClO_4^-, and PF_6^- and not with larger ones as bis (trifluoromethylsulfonyl)amide Tf_2N^-, among others. This has been explained as due to the proximity of the counterion to the monolayer-protected layer (MPC) that allowed the alkanethiolate layer to get charge compensation, and this was proposed as a new way to modulate the electronic-charging response of the film [78]. Monolayer metal deposition at the electrochemical interface has proved the halide–metal interaction [79].

Electrochemiluminescence and Spectroelectrochemistry

Electrochemiluminescence (ECL) consists of the radiative deactivation of excited states that have been generated electrochemically. In QDs, this process can occur via an annihilation process involving only QD radical ions (*QD-annihilation-based* ECL), or it can require a coreactant (*coreactant-based ECL*), both schematized in Fig. 12. In *QD-annihilation-based ECL*, under electrochemical conditions, an individual QD can accept an electron in its conduction band while another donates an electron from its valence band, thus leading to the QD radical anion/QD radical cation couple (QD^-/QD^+). Subsequent collision of the radicals produces the ground state of one of them and the excited state (QD*) of the other, which finally reaches the ground state after emitting light. The stepwise removal or addition of charge from QDs by an electrochemical method can give information on the energy needed for electron transfer and, consequently, for ECL emission. This type of electrochemiluminescence has been exhibited by QDs with a superlattice structure, but it has not been detected in QDs capped with electrochemically inert ligands, such as mercaptoalkanes.

In *coreactant-based ECL*, a coreactant (CR) and a QD can be electrochemically reduced, eventually leading to an oxidized species (S_{Ox}) and QD^-, and then the S_{Ox}/QD^- couple reacts to lead to an unreactive product (S_F) and the QD excited state (QD*), which partially decays via a radiative process. Alternatively, the CR

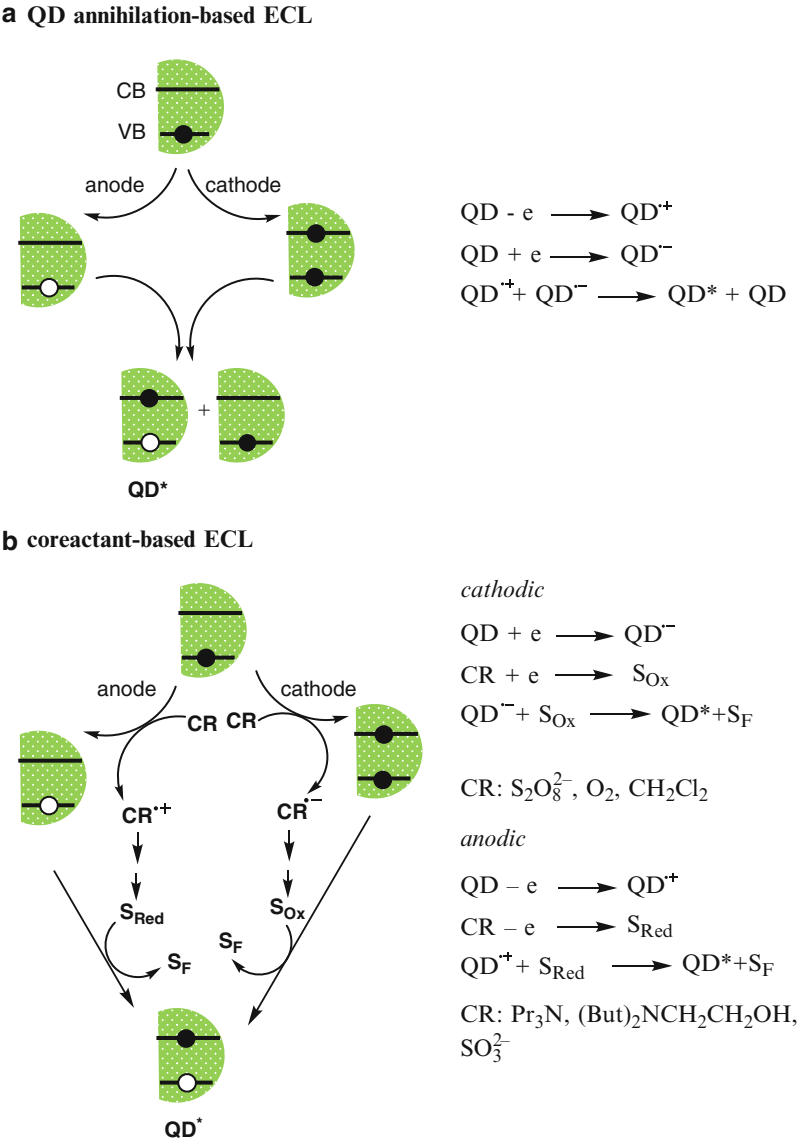

Fig. 12 Schemes for (**a**) annihilation-based and (**b**) coreactant based ECL

and the QD are electrochemically oxidized, eventually leading to a reduced form (S_{Red}) and QD^+ and then the S_{Red}/QD^+ couple reacts yielding QD*. These processes are further classified as cathodic- and anodic-based ECL depending on the role of the CR as an oxidant or reductant, respectively, that will rely on the oxidation or reduction potential of the resulting S_{Ox} or S_{Red} intermediate. The coreactant-based ECL possesses several advantages over the QD annihilation-based ECL, in

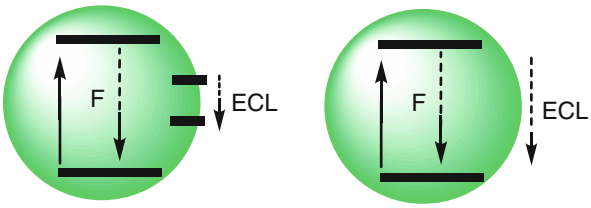

Fig. 13 Schemes for band gap-based ECL (*left*) and surface state-based ECL (*right*)

particular when either the QD radical cation or the radical anion is not quite stable or the electrode or the solvent has a narrow potential window so that neither of these radical ions can be generated.

The coreactants can be (i) amines, such as tri-*n*-propylamine and triethanolamine); (ii) peroxides, such as O_2, H_2O_2, $S_2O_8^{2-}$; (iii) other species like SO_3^{2-}, CH_2Cl_2; and (iv) other nanoparticles. A number of considerations have to be taken into account for choosing the right coreactant, such as its solubility, stability, electrochemical activity, direct ECL, as well as suitability to be easily oxidized or reduced at or near the electrode and its capacity to leading rapidly to the corresponding reactive intermediate.

There are a considerable number of examples of ECL in QDs such as CdSe, CdS, and CdTe. It has been recently demonstrated that water dispersible, blue-luminescent graphene QDs exhibit an ECL behavior similar to CdSe QDs. These QDs present anodic ECL when using H_2O_2 as the coreactant, and this emission is strong and appears at low potential (ca. 0.4 V vs. Ag/AgCl) [80].

The ECL emission can originate from recombination of an electron and a hole at the conduction and valence band edges of the QD core, respectively, and it matches the band-edge fluorescence and is size dependent. Alternatively, the ECL can involve transition levels caused by defect states at the QD surface, and, consequently, energy relaxation and recombination dynamics in QDs strongly depend on passivation of the QD surface (Fig. 13). Consequently, the QD- based ECL can be classified as band gap or surface state ECL. Because electron/hole injection in QDs is assumed to occur via the surface states, the surface state-based ECL has been considered as the main process for QD ECL, but there are increasing reports showing that QDs can exhibit band gap-based ECL or both types of ECL, the contribution of the first increasing by progressive passivation of the QD surface. In addition, it has to be taken into account that the introduction of coreactants can have an impact on surface state-based QD ECL and a "dual peak" can appear.

Metallic nanoparticles can be used to improve the ECL performance of QDs due to their excellent conductivity. Thus, they can reduce the electron-relay barrier between the QD and the electrode, accelerating the electron/hole injection, thus enhancing ECL intensity and moving ECL onset and the peak potential toward zero. For example, ECL of CdS–CdSe QDs was drastically enhanced by placing a large number of silica-coated AuNPs on their surface [81].

Furthermore, silver and gold nanoclusters can also exhibit their own ECL. Metal nanoclusters differ from their corresponding nanoparticles in that the continuous

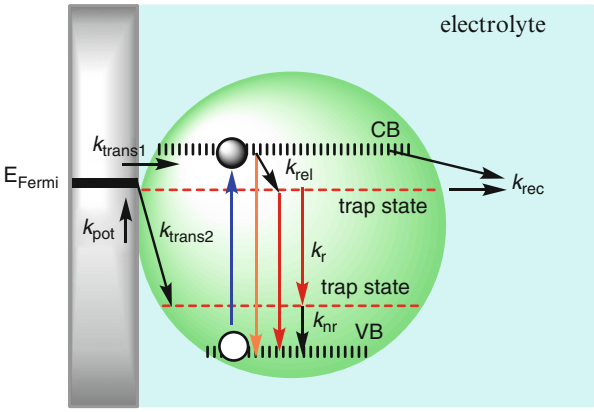

Fig. 14 Schematic representation of the plausible processes occurring after QD illumination under potentiostatic control

density of states breaks into discrete energy levels and as a consequence they can exhibit molecule-like properties, such as luminescence. Thus, nanoclusters with a small number of Ag atoms can show a considerable fluorescence quantum yield as well as ECL under strong cathodic polarization using $K_2S_2O_8$ as the coreactant. The ECL spectrum of the nanoclusters matched that of their photoluminescence [82].

In the case of gold, Au_{25} nanoclusters protected by bovine serum albumin can exhibit ECL by using triethylamine as the coreactant, but in this case the ECL spectrum matched the surface-state fluorescence that appeared as a weak shoulder on the main peak in the Au_{25} nanocluster fluorescence spectrum [83]. By contrast, the ECL spectrum of similar Au_{25} nanoclusters immobilized on hydroxylated indium tin oxide (ITO) and using $K_2S_2O_8$ as the coreactant was similar to that of the photoluminescence spectrum [83].

These optical spectroelectrochemistry techniques have been recently used to obtain information on the relationship between the emissive properties of QDs and their intrinsic structure features. Thus, the absolute energetic position of trap levels can be determined by using an electrochemical method which is particularly useful for QD electrodes [84], once the energy of the bandgap edges is known. It consists of the control of the population of the energy states involved in fluorescence by potentiostatic control of the Fermi level in the material, thus enhancing or quenching the fluorescence depending on the energy state involved (Fig. 14). It should be emphasized that semiconductor materials possess defect states that originate from substitutional and interstitial impurities, divacancies, surface reactions, etc., resulting from their synthesis. For example, the absolute energetic position of the trap levels involved in the green fluorescence of thin films of ZnO QDs has been determined [84]. Under illumination, the Fermi level in the QD increases due to the increase of electrons in the CB. Competitively with the recombination with the VB holes, the CB electrons can relax into a lower-lying, electron-acceptor trap state (k_{rel}) and by recombination with the electrolyte (k_{rec}) from the CB or from the trap state. Under potentiostatic control, the trap emission can increase due to the population of the trap state (k_{trans1}), subsequently increasing the probability for radiative and

non-radiative recombination (k_r and k_{nr}, respectively). If $k_r >> k_{nr}$ and $k_r > k_{rec}$ an increase in the surface-state emission would be observed. As a result, it was demonstrated that the green fluorescence of thin films of ZnO QDs is caused by a transition from an upper trap level, at 0.35 ± 0.03 eV below the conduction band edge, to a deep trap within the bandgap and that the position of this upper level shifts with the size of the QD in the same way as the conduction band. Although this did not happen in these QDs, this method could alternatively induce the quenching of the QD fluorescence by applying more negative potentials than that of the upper trap level via competitive population of a deep, electron-acceptor trap-state (k_{trans2}), if this process is fast enough.

In addition, optical spectroelectrochemistry techniques have been applied to obtain information on the basis of QD photoluminescence blinking, which is a random switching between states of high (ON) and low (OFF) emissivities. The OFF periods are often explained by using a charging model (additional charge causing photoluminescence quenching by non-radiative recombination, Auger mechanism). However, time-resolved photoluminescence studies of individual QDs have been carried out by controlling the QD charging electrochemically and suggest that there are two types of blinking (i) A-type blinking (Auger mechanism) in which the lower photoluminescence intensity is accompanied by a short luminescence lifetime and (ii) B-type blinking, due to charge fluctuations in the electron-accepting surface states, in which the lower emission is not accompanied by a significant change in the QD emission lifetime. In B-type blinking, unoccupied surface states intercept hot electrons before they relax into emitting core states (Fig. 15). Both blinking mechanisms can be suppressed by application of the appropriate potential.

These types of studies have been conducted on single CdSe/CdS QDs, by performing time-tagged, time-resolved, single photon counting measurements in a three-electrode electrochemical cell. At $E = 0$ V and $E = +0.8$ V, periods of low luminescence intensity and a considerable shortening of lifetime was observed. These effects can be attributed to a low Fermi level, increasing the relative time spent by the trap in the unoccupied state, and consequently having the capacity of trapping hot electrons which eventually recombine non-radiatively with a VB hole, thus resulting in a neutral QD. These B-type blinking events usually coexist with A-type fluctuations. For negative potentials ($E = -1$ V), the fluorescence lifetime was typical of a neutral exciton, but the blinking was suppressed by increasing the energy of the Fermi level that led to population of the trap states. At more negative potentials, the photoluminescence decay became biexponential and the QD lifetime was drastically reduced. This has been attributed to charging the QD with extra electron and emission from negative trions.

The different origin of A- and B-type blinking of QDs became patent by increasing the shell thickness. While type-B blinking is reduced and even suppressed, by adding an increasing number of shell monolayers, A-type can still be detected in the case of highly thick shells. Interestingly, it has been shown that hollow spherical CdSe assemblies generate intense ECL using persulfate as the coreactant. The aggregation has a protective effect on the electrogenerated reduced species, facilitating a more competitive radiative charge recombination process [85].

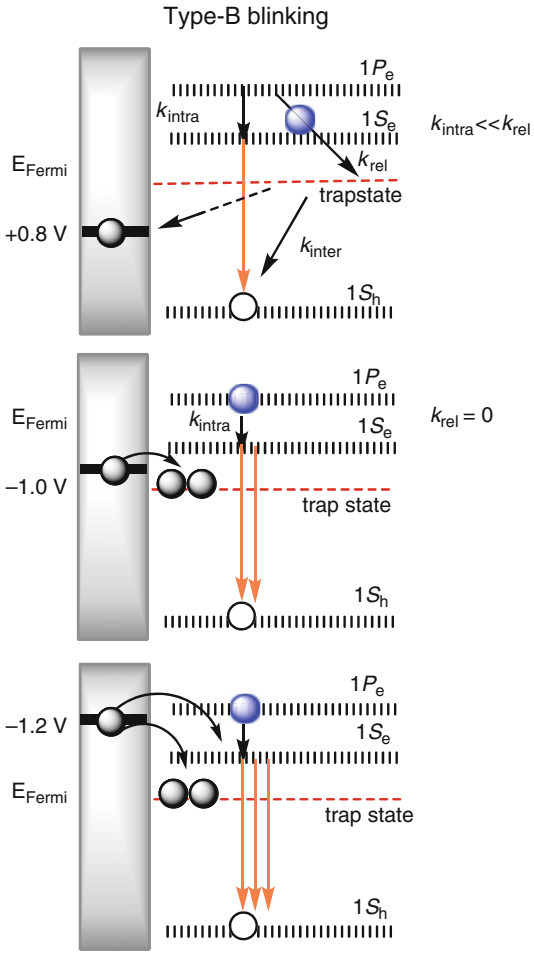

Fig. 15 Schematic representations for the processes involved in B-type binking

Graphene-QD composites are being used increasingly for accelerating the electron transfer on the electrode surface and amplifying the ECL of QDs [86, 87]. Moreover, ECL immunoassays have become a smart analytical tool; they make use of ECL-active species as labels on biological molecules and of the high affinity of antibodies for their corresponding antigens (Fig. 16). Thus, it has recently been shown that ZnO nanospheres can be used to increase the loading of CdTe QDs, leading to QD/carrier nanocomposites with higher ECL intensity and better ECL stability than that of the CdTe QDs [88]. For the construction of the ECL immunosensor, the biomolecule is immobilized on a sensing surface (conducting bridge). For example, Au-Pt bimetallic nanoparticles are deposited on a glassy carbon electrode and the resulting nanocomposite is more effective than pure Pt nanoparticles for accelerating the electron transfer.

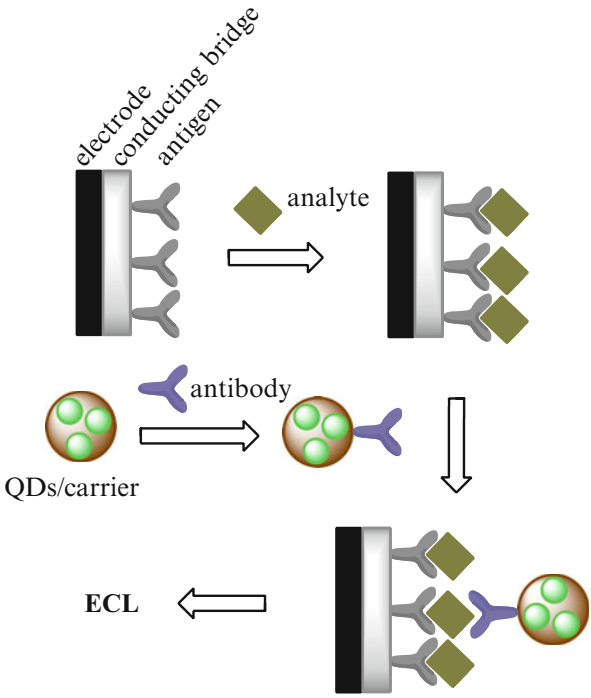

Fig. 16 Scheme for ECL immunoassays based on labeling of biological molecules

Finally, upconverting nanoparticles (UCNPs), such as $NaYF_4/Yb^{3+},Er^{3+}$, are peculiar ECL nanoemitters, since they exhibit anti-Stokes fluorescence. Examples of UCNP ECL are rare, but recently UCNP@SiO_2 core-shell nanohybrids modified with polyoxometalates have shown ECL dependence on the applied potential [89] whereas there are ECL biosensors whose sensing is based on the combination of ECL and energy transfer (ECL-ET). Thus, the ECL of CdSeTe/CdS/ZnS QDs can be modulated in the presence of Au nanorods and this strategy has been applied to build a sensitive ECL-ET based sensor of a biomarker [90].

Nanoparticles as Redox Mediators

Electrocatalytic Effects

Electrocatalysis has been performed by attaching nanoparticles to the electrode surfaces, forming different types of films/deposits/nanocomposites. The nanoparticle-modified electrodes have several advantages compared to bulk electrodes, such as fast electron transfer kinetics, lower overpotential, and enhancement of electro-active surface area, thus facilitating kinetically hindered redox reactions.

Metal nanoparticles such as Pt, Pd, Au and Fe have demonstrated good electrocatalytic performance toward different electrochemical processes [91].

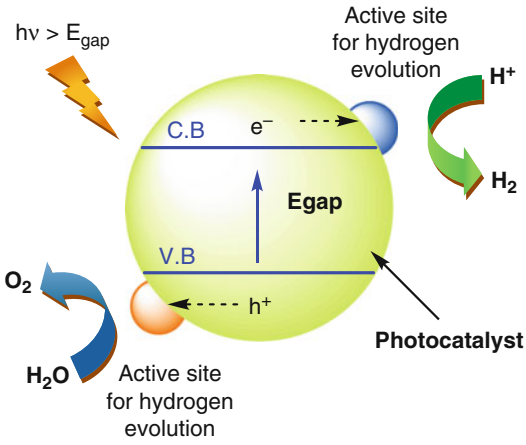

Fig. 17 Scheme for photoelectrocatalytic water splitting using semiconductor nanoparticles by means of the semiconductor liquid junction approach [102]

Electrochemical reduction of oxygen dissolved in aqueous electrolytes (oxygen reduction reaction, ORR) can be taken as a paradigmatic example of reactions catalyzed by metal nanoparticles [92]. The electrocatalytic effect exerted by gold nanoparticles on ORR depends on the shape and size of the NPs [93, 94], and the number of electrons exchanged during the ORR is dependent on the nanoparticle shape [95]. The efficiency of the catalytic process can be improved by combination with other nanomaterials and may be photochemically assisted. Semiconductor nanoparticles, such as TiO_2, have shown interesting photoelectrocatalytic activity [91].

A plethora of multifunctional electro- and photoelectrocatalysts have been reported with applications in the fields of sensing, fuel cells, and water splitting. Among them are bimetallic nanoparticles with different core-shell compositions and architecture [95, 96] and nanocomposites of metal nanoparticles with semiconductor materials. In addition, both types of nanoparticles can be associated with other material, such as polymers or graphene to form nanocomposites which present catalytic and sensing applications, thus improving those displayed by the separated components. The electrocatalytic performance of metal nanoparticles on different kinds of graphite surfaces has recently been reviewed [96, 97]. Regarding the nanoparticle-polymer combination, nanocomposites of poly(amidoamine)-encapsulated platinum nanoparticles and phosphotungstic acid have been used as an electrocatalyst for the hydrogen evolution reaction (HER) [98].

An important group of applications deals with photoelectrocatalytic water splitting where either photovoltaic cells or semiconductor-liquid junctions, or both, have been combined [99]. In general, water splitting can be achieved effectively when a cocatalyst is added together with the photocatalyst, for example, a metal and semiconductor nanoparticle [100, 101]. Figure 17 shows a scheme for the photoelectrochemical water splitting by means of a semiconductor-liquid junction cell. The photocatalytic activity of the process depends on the physicochemical properties of the photocatalyst, the nature of the active sites (usually known as cocatalyst), and the conditions of the reaction [102].

Another interesting application of electrocatalysis and photoelectrocatalysis is that of removing of organic pollutants via electrooxidation. Among different compositional and architectural varieties, Cu_2O/TiO_2 composite nanotubes improve the separation of photogenerated electrons and holes so that Cu_2O/TiO_2 heterojunction photoelectrodes exhibit a more effective photoconversion capability than TiO_2 nanotubes alone for oxidative degradation of pollutant probes [103].

Multifunctional photocatalysts are receiving considerable attention because of their potential ability for promoting oxidation and reduction processes simultaneously. In particular, metal and semiconductor nanoparticles have been anchored to different carbon nanostructures, such as single or multiwall carbon nanotubes and graphene oxide/reduced graphene oxide. Reduced graphene oxide has been used as a two dimensional support for semiconductor nanoparticles like TiO_2 on one side of the material and the metal ions on the other. After light irradiation the electrons generated in the semiconductor are transported through the graphene to reduce silver ions into silver nanoparticles localized on the other side of the material [104, 105].

Sensing at Nanoparticulate Films and Composites

Electrocatalysis can also be used for sensing purposes. The development of an electrochemical sensor has the following steps (i) synthesis of the nanoparticle, (ii) modification of the electrode with the nanoparticles, and (iii) characterization of the nanoparticle-modified electrodes. After the synthesis of the nanoparticle, following well-known methodologies, the electrode surface should be modified with those nanoparticles using different physical or chemical techniques, such as a simple mixture of the NPs with additives (enzymes), solvent evaporation, chemical covalent bonding, NP growth in the sol–gel network, electro-aggregation, and so on. Electrodeposition of the nanoparticle on the electrode surface seems to be one of the most used techniques due to their simplicity; however, one limitation is the size distribution of the NP, which depends on the deposition time, deposition potential, electrolyte solution and salt concentration, and the non-uniform distribution of the nanoparticles on the electrode. The previous modification of the nanoparticle surface can overcome this problem. The functionalization of nanoparticles with molecules or biomolecules plays a key role in their sensing applications because the functionality can induce changes on the photophysical properties of the nanoparticle and modify their immobilization on the electrode [106, 107].

For instance, the organothiolate capped Au_{25} nanoparticle clusters have good electrocatalytic activity toward the electrochemical oxidation of ascorbic and uric acids, where Au_{25} plays a dual role as an electronic conductor and redox mediator. Electron transfer studies showed a correlation between the electronic conductivity of Au nanoparticles and the sensing sensitivity. The proposed mechanism is initiated by the oxidation of Au nanoparticles (Au_{25}^{-}) to Au_{25}^{0}, which produces the electrocatalytical oxidation of the analyte and the regeneration of the nanoparticles, increasing the anodic current as the analyte concentration increases.

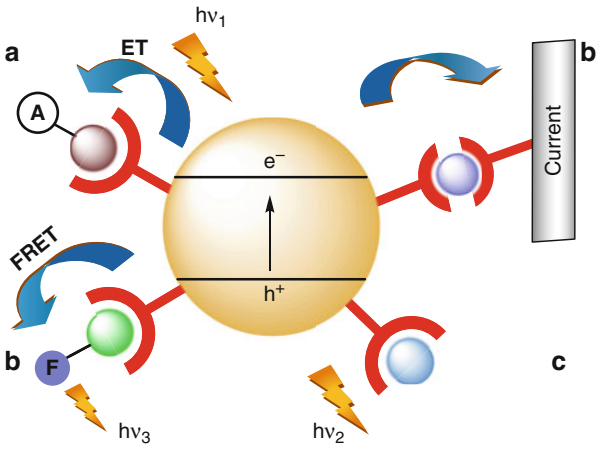

Fig. 18 Schematic representation of a QD-based sensor using: (**a**) electron transfer to an acceptor molecule, (**b**) photocurrent generation, (**c**) fluorescence, and (**d**) FRET

The electrocatalytic activity of the Au_{25} NPs has been attributed to the electron-deficient Au_{12} shell and to the low-coordinated surface gold atoms [108].

Direct DNA detection is usually obtained following the redox behavior of bases or sugar residues; however, indirect detection can be determined by using nanoparticles. The DNA hybridization sensing has been studied from the electrochemical detection of DNA by the catalytic silver cluster formed on the DNA strand. The Ag^+ ions on the immobilized DNA are subsequently reduced by hydroquinone to form the aggregates that after acidic solution addition are solubilized and detected by stripping potentiometric detection. This is a powerful electroanalytical technique for trace metal measurements, attributed to the built-in preconcentration step as a consequence of the metal accumulation in the working electrode. Detection of DNA, protein, and biomolecules of interest by using enzyme-nanoparticle hybrids has also been reviewed [109]. In addition, enzyme/protein –nanoparticle based sensors have also been used for sensing of small molecules, such as peroxide, colesterol, glucose, phenolic compounds, gallic acid, and others. Moreover, the detection of gaseous components that can be responsible of air pollution, such as H_2S, ozone, H_2, NO_x, NH_3, is currently receiving a great interest. Chemical modification of nanoparticles can help to prepare nanoparticle-modified electrodes for gas sensing [110]. Also relevant is the detection of biological systems used for clinical diagnostic (cancer biomarkers, proteins, bacterias, and cancer cells) by using sensors based on gold nanoparticles [111].

Nucleic acid/semiconductor nanoparticle hybrid systems have been used for optical and electrochemical sensing taking advantage of the recognition and catalytic properties of nucleic acid and the photophysical properties of QDs [112]. The strategy of detection can be based on different mechanisms, such as fluorescence resonance energy transfer (FRET), chemiluminiscence energy transfer, electron transfer, among others (Fig. 18).

In general, the design of polyelectrolyte gold nanoparticule composite films requires to consider the following factors (i) the nanoparticle film density,

(ii) the electronic inter-nanoparticle coupling and also between the film assembly, (iii) the analyte accessibility within the film to the electrode, and (iv) the stabilizer layer of the nanoparticle [113].

Interestingly, synergetic effects obtained in a variety of nanocomposites involving different kinds of nanoparticles, for instance, graphene-Au nanoparticles [114], are extensively studied for sensing purposes. These include a variety of nanoarchitectures (core and core@shell nanoparticles, nanorods, nanowires, etc.) able to be deposited on inert electrodes displaying voltammetric and amperometric sensing with enhanced sensitivity and selectivity with respect to the unmodified electrodes. Similar strategies are being developed in the case of quantum dots, accompanied by functionalization and doping [115], with applications in biochemical [116] and biomedical [117] analysis.

Nanoparticle modified-electrode is a promising methodology in electrochemistry for future miniaturization of opto-electronic and for the development of electrochemical bio-nanochip. More specific and selective sensors would benefit from the design of new hybrid materials and better understanding of the detection principle and performance of electrochemical techniques.

Conclusion

Metal and semiconductor nanoparticles possess distinctive electrochemical and photoelectrochemical responses to that of their macroscopic equivalents. Electrochemical techniques can give significant information on the structure, composition, and quantum confinement effects of microparticulate systems reflected in different electrochemical regimes. Voltammetric features provide information on bandgap energy, the position of conduction and valence band edges, and defect sites of the nanoparticulate systems, as well as on the inter-particle interaction and binding to capping ligands.

Electrocatalytic and photoelectrocatalytic phenomena involving metal nanoparticles and quantum dots, as well as different nanostructured materials with a variety of architectures, can be used for a variety of applications from water splitting to removal of pollutants and they are extensively used for electrochemical sensing. In summary, both from the fundamental and applied point of view, the electrochemistry of nanoparticulate systems can be considered as an important research field whose expansion will probably continue during the next years.

References

1. C.N.R. Rao, G.U. Kulkarni, A. Govindaraj, B.C. Satishkumar, P.J. Thomas, Pure Appl. Chem. **72**, 21–33 (2000)
2. A. Eftekhari (ed.), *Nanostructured Materials in Electrochemistry* (Wiley, Weinheim, 2008)
3. A. Henglein, Top. Curr. Chem. **143**, 113–180 (1988)
4. A. Henglein, Chem. Rev. **89**, 1861–1873 (1989)

5. A. Henglein, J. Phys. Chem. **83**, 2209–2216 (1979)
6. J. Kiwi, M. Grätzel, J. Am. Chem. Soc. **101**, 7214–7217 (1979)
7. R.W. Murray, Chem. Rev. **108**, 2688–2720 (2008)
8. M. Amelia, C. Lincheneau, S. Silvi, A. Credi, Chem. Soc. Rev. **41**, 5728–5743 (2012)
9. A.J. Bard, Z. Ding, N. Myung, Struct. Bond. **118**, 1–57 (2005)
10. W. Kucur, W. Bücking, T. Nann, Microchim. Acta **160**, 299–308 (2008)
11. D.S. Miller, A.J. Bard, G. McLendon, J.J. Ferguson, J. Am. Chem. Soc. **103**, 5336–5341 (1981)
12. G. Schmid, U. Giebel, W. Hunter, A. Schwenk, Inorg. Chim. Acta **85**, 97–102 (1984)
13. M.G. Bawendi, M.L. Steigerwald, L.E. Brus, Ann. Rev. Phys. Chem. **41**, 477–496 (1990)
14. M.J. Weaver, X. Gao, J. Phys. Chem. **97**, 332–338 (1993)
15. G. Chumanov, K. Sokolov, B.W. Gregory, T.M. Cotton, J. Phys. Chem. **99**, 9466–9471 (1995)
16. K.C. Grabar, R.G. Freeman, M.B. Hommer, M.J. Natan, Anal. Chem. **67**, 735–743 (1995)
17. T. Ung, M. Giersign, D. Dunstan, P. Mulvaney, Langmuir **13**, 1773–1782 (1997)
18. R.S. Ingram, M.J. Hostetler, W.R.W. Murray, T.G. Schaaf, J. Khoury, R.L. Whetten, T.P. Bigioni, D.K. Githrie, P.N. First, J. Am. Chem. Soc. **119**, 9279–9280 (1997)
19. S. Chen, R.S. Ingram, M.J. Hostetler, J.J. Pietron, R.W. Murray, T.G. Schaaff, J.T. Khoury, M.M. Alvarez, R.L. Whetten, Science **280**, 2098–2101 (1998)
20. M.O. Finot, G.D. Braybrook, M.T. McDermott, J. Electroanal. Chem. **466**, 234–241 (1999)
21. A. Doménech-Carbó, J. Labuda, F. Scholz, Pure Appl. Chem. **85**, 609–631 (2013)
22. R. Tel-Vered, A.J. Bard, J. Phys. Chem. B **110**, 25279–25287 (2006)
23. Y. Gründer, H.L.T. Ho, J.F.W. Mosselmans, S.L.M. Schroeder, R.A.W. Dryfe, Phys. Chem. Chem. Phys. **13**, 15681–15689 (2011)
24. A.J. Bard, M.V. Mirkin (eds.), *Scanning Electrochemical Microscopy*, 2nd edn. (CRC Press, Boca Raton, 2012)
25. D.G. Georgnopoulou, M.V. Mirkin, R.W. Murray, Nano Lett. **4**, 1763–1767 (2004)
26. R.G. Fedorov, D. Mandler, Phys. Chem. Chem. Phys. **15**, 2725–2732 (2013)
27. X. Shan, U. Patel, S. Wang, R. Iglesias, N. Tao, Science **327**, 1363–1366 (2010)
28. K. Huang, A. Agnès, M.A. Bahri, C. Demaille, ACS Nano **7**, 4151–4163 (2013)
29. D.J. Norris, A.L. Efros, M. Rosen, M.G. Bawendi, Phys. Rev. B **53**, 16347–16354 (1996)
30. C. Burda, X. Chen, R. Narayanan, M.A. El-Sayed, Chem. Rev. **105**, 1025–1102 (2005)
31. A.M. Smith, S. Nie, Acc. Chem. Res. **43**, 190–200 (2010)
32. B.M. Quinn, P. Lijeroth, V. Ruiz, T. Laaksonen, K. Kontturi, J. Am. Chem. Soc. **125**, 6644–6645 (2003)
33. G.C. Lica, B.S. Zelakiewicz, Y.Y. Tong, J. Electroanal. Chem. **554**, 127–132 (2003)
34. R.L. Wolfe, R.W. Murray, Anal. Chem. **78**, 1167–1173 (2006)
35. M.R. Branham, A.D. Douglas, A.J. Mills, J.B. Tracy, P.S. White, R.W. Murray, Langmuir **22**, 11376–11383 (2006)
36. L.D. Menard, S.-P. Gao, H. Xu, R.D. Twesten, A.S. Harper, Y. Song, G. Wang, A.D. Douglas, Y.C. Yang, A.I. Frenkel, R.G. Nuzzo, R.W. Murray, J. Phys. Chem. B **110**, 12874–12883 (2006)
37. S. Yang, D. Prendergast, J.B. Neaton, Nano Lett. **12**, 383–388 (2012)
38. A.C. Templeton, W.P. Wuelfing, R.W. Murray, Acc. Chem. Res. **33**, 27–36 (2000)
39. S. Devarajan, S. Sampath, Chem. Nanomater. **2**, 646–687 (2004)
40. D.T. Miles, R.W. Murray, Anal. Chem. **75**, 1251–1257 (2003)
41. J.F. Hicks, A.C. Templeton, S. Chen, K.M. Sheran, R. Jasti, R.W. Murray, J. Debor, T.G. Schaaff, R.L. Whetten, Anal. Chem. **71**, 3703–3711 (1999)
42. G. Makov, A. Nitzan, L.E. Brus, J. Chem. Phys. **88**, 5076–5085 (1988)
43. J.P. Perdew, Phys. Rev. B **36**, 6175–6180 (1988)
44. J.J. Pietron, J.F. Hicks, R.W. Murray, J. Am. Chem. Soc. **121**, 5565–5570 (1999)
45. S.J. Green, J.J. Stokes, M.J. Hoestetler, J. Pietron, R.W. Murray, J. Phys. Chem. B **101**, 2663–2668 (1997)
46. S.J. Chen, J. Electroanal. Chem. **574**, 153–165 (2004)

47. D. Lee, R.L. Donkers, G.L. Wang, A.S. Harper, R.W. Murray, J. Am. Chem. Soc. **126**, 6193–6199 (2004)
48. T. Iwasa, K. Nobusada, Chem. Phys. Lett. **441**, 268–272 (2007)
49. Y. Yang, S. Chen, Nano Lett. **3**, 75–79 (2003)
50. G. Schmid, Chem. Rev. **92**, 1409–1418 (1992)
51. A. Doménech-Carbó, E. Coronado, P. Díaz, A. Ribera, Electroanalysis **22**, 293–302 (2010)
52. M. Grden, J. Kotowski, A. Czerwinski, J. Solid State Electrochem. **4**, 273–278 (2000)
53. S.N. Inamdar, P.P. Ingole, S.K. Haram, Chem. Phys. Chem **9**, 2574–2579 (2008)
54. E. Kukur, J. Riegler, G.A. Urban, T. Nann, J. Chem. Phys. **119**, 2333–2337 (2003)
55. S. Impellizzeri, S. Monaco, I. Yildiz, M. Amelia, A. Credi, F.M. Raymo, J. Phys. Chem. C **114**, 7007–7013 (2010)
56. A.K. Gooding, D.E. Gomez, P. Mulvaney, ACS Nano **2**, 669–676 (2008)
57. D. Dorokhin, N. Tomeczak, D.N. Reihoudt, A.H. Velders, G.J. Vancso, Nanotechnology **21**, 285703 (2010)
58. J. Aguilera-Sigalat, V.F. Pais, A. Doménech-Carbó, U. Pischel, R.E. Galian, J. Pérez-Prieto, J. Phys. Chem. C **117**, 7365–7375 (2013)
59. S.K. Poznyak, N.P. Osipovich, A. Shavel, D.V. Talapin, M. Gao, A. Eychmüller, N. Gaponik, J. Phys. Chem. B **109**, 1094–1100 (2005)
60. W.J. Plieth, J. Phys. Chem. **86**, 3166–3172 (1982)
61. P.L. Redmon, A.J. Hallock, L.E. Brus, Nano Lett. **5**, 131–135 (2005)
62. Kh.Z. Brainina, L.G. Galperin, A.L. Galperin, J. Solid State Electrochem. **14**, 981–988 (2010)
63. Kh.Z. Brainina, L.G. Galperin, E.V. Vikulova, N.Yu. Stozhko, A.M. Murzakaev, O.R. Timoshenkova, Yu.A. Kotov, J. Solid State Electrochem. **15**, 1049–1056 (2011)
64. Kh.Z. Brainina, L.G. Galperin, L.A. Piankova, N.Yu. Stozhko, A.M. Murzakaev, O.R. Timoshenkova, J. Solid State Electrochem. **15**, 2469–2475 (2011)
65. Kh.Z. Brainina, L.G. Galperin, T.Yu. Kiryuhina, A.L. Galperin, N.Yu. Stozhko, A.M. Murzakaev, O.R. Timoshenkova, J. Solid State Electrochem. **16**, 2365–2372 (2012)
66. L. Tang, X. Li, R.C. Cammarata, C. Friesen, K. Sieradzki, J. Am. Chem. Soc. **132**, 11722–11726 (2010)
67. M. Thompson, R.G. Compton, Chem. Phys. Chem. **7**, 1964–1970 (2006)
68. T.J. Davies, R.G. Compton, J. Electroanal. Chem. **585**, 63–82 (2005)
69. T.J. Davies, C.E. Banks, R.G. Compton, J. Solid State Electrochem. **9**, 797–808 (2005)
70. Y.G. Zhou, N.V. Rees, R.G. Compton, Angew. Chem. Int. Ed. **50**, 4219–4221 (2011)
71. H.S. Toh, C. Batchelor-McAuley, K. Tschulik, M. Uhlemann, A. Crossleyc, R.G. Compton, Nanoscale **5**, 4884–4893 (2013)
72. Y.G. Zhou, N.V. Rees, R.G. Compton, Chem. Phys. Lett. **511**, 183–186 (2011)
73. Y.G. Zhou, N.V. Rees, R.G. Compton, Chem. Phys. Chem. **12**, 2085–2087 (2011)
74. X. Xiao, A. Bard, J. Am. Chem. Soc. **129**, 9610–9612 (2007)
75. X. Xiao, F.R.F. Fan, J. Zhou, A.J. Bard, J. Am. Chem. Soc. **130**, 16669–16677 (2008)
76. S.J. Kwon, F.R.F. Fan, A.J. Bard, J. Am. Chem. Soc. **132**, 13165–13167 (2010)
77. S.J. Kwon, H. Zhou, F.-R.F. Fan, V. Vorobyev, B. Zhang, A.J. Bard, Phys. Chem. Chem. Phys. **13**, 5395–5402 (2011)
78. W. Li, B. Su, Electrochem. Commun. **33**, 27–30 (2013)
79. Y. Gründer, P. Thompson, A. Brownrigg, M. Darlington, C.A. Lucas, J. Phys. Chem. C **116**, 6283–6288 (2012)
80. J. Lu, M. Yan, L. Ge, S. Ge, S. Wang, J. Yan, Biosens. Bioelectron. **47**, 271–277 (2013)
81. G.F. Jie, P. Liua, S.S. Zhang, Chem. Commun. **46**, 1323–1325 (2010)
82. I. Díez, M. Pusa, S. Kulmala, H. Jiang, A. Walther, A.S. Goldmann, A.H.E. Müller, O. Ikkala, R.H.A. Ras, Angew. Chem. Int. Ed. **48**, 2122–2125 (2009)
83. L. Li, H. Liu, Y. Shen, J. Zhang, J.J. Zhu, Anal. Chem. **83**, 661–665 (2011)
84. T.J. Jacobsson, T. Edvinsson, J. Phys. Chem. C **117**, 5497–5504 (2013)
85. B. Liu, T. Ren, J.R. Zhang, H.Y. Chen, J.J. Zhu, C. Burda, Electrochem. Commun. **9**, 551–557 (2007)

86. Z. Guo, T. Hao, S. Du, B. Chen, Z. Wang, X. Li, S. Wang, Biosens. Bioelectron. **44**, 101–107 (2013)
87. W. Li, W. Dai, L. Ge, S. Ge, M. Yan, J.J. Yu, Inorg. Organomet. Polym. **23**, 719–725 (2013)
88. F. Liu, Y. Zhang, C. Chu, J. Lu, J. Yu, X. Song, *Monatshefte für Chemie – Chemical Monthly* (Springer, Vienna, 2013)
89. Y. Zhai, C. Zhu, J. Ren, E. Wang, S. Dong, Chem. Commun. **49**, 2400–2402 (2013)
90. I. Li, Y. Chen, Q. Lu, J. Ji, Y. Shen, M. Xu, R. Fei, G. Yang, K. Zhang, J.R. Zhang, J.J. Zhu, Sci. Rep. **3**, 1529 (2013). doi:10.1038/srep01529
91. Z.Y. Zhou, N. Tian, J.T. Li, I. Broadwell, S.G. Sun, Chem. Soc. Rev. **40**, 4167–4185 (2011)
92. J. Xu, W. Huang, R.L. McCreery, J. Electroanal. Chem. **410**, 235–242 (1996)
93. J. Hernández, J. Solla-Gullón, E. Herrero, J. Electroanal. Chem. **574**, 185–196 (2004)
94. A.J. Wain, Electrochim. Acta **92**, 383–391 (2013)
95. C.M. Sánchez-Sánchez, F.J. Vidal-Iglesias, J. Solla-Gullón, V. Montiel, A. Aldaz, J.M. Feliu, E. Herrero, Electrochim. Acta **55**, 8252–8257 (2010)
96. P. Mayer, R. Holze, J. Solid State Electrochem. **5**, 402–411 (2001)
97. O.A. Petrii, J. Solid State Electrochem. **12**, 609–642 (2008)
98. L. Sun, D. Vu, J.A. Cox, J. Solid State Electrochem. **12**, 816–822 (2005)
99. A. Currao, Chimia **61**, 815–819 (2007)
100. J. Yu, L. Qi, M. Jaroniec, J. Phys. Chem. C **114**, 13118–13125 (2010)
101. Y. Lai, J. Gong, C. Lin, Int. J. Hydrogen. Energy **37**, 6438–6446 (2011)
102. K. Maeda, K. Domen, J. Phys. Chem. Lett. **1**, 2655–2661 (2010)
103. M. Wang, L. Sun, Z. Lin, J. Cai, K. Xie, C. Lin, Energy Environ. Sci. **6**, 1211–1220 (2013)
104. I.V. Lightcap, T.H. Kosel, P.V. Kamat, Nano Lett. **10**, 577–583 (2010)
105. P.V. Kamat, J. Phys. Chem. Lett. **3**, 663–672 (2012)
106. L. Rassaei, M. Amiri, C.M. Cirtiu, M. Sillanpää, F. Marken, M. Sillanpää, Trends Anal. Chem. **30**, 1704–1715 (2011)
107. S. Jiang, K.Y. Win, S. Liu, C.P. Teng, Y. Zheng, M.-Y. Han, Nanoscale **5**, 3127–3148 (2013)
108. S.S. Kumar, K. Kwak, D. Lee, Anal. Chem. **83**, 3244–3247 (2011)
109. J. Wang, E. Katz, I. Willner (eds.), *Bioelectronics* (Wiley, Weinheim, 2005)
110. F. Wang, S. Hu, Microchim. Acta **165**, 1–22 (2009)
111. P. Chandra, J. Singh, A. Singh, A. Srivastava, R.N. Goyal, Y.B. Shim, J. Nanopart. Art ID: 535901, 12 p (2013)
112. R. Freeman, J. Girsh, I. Willner, Appl. Mater. Interfaces **5**, 2815–2834 (2013)
113. A.R. Schmidt, N.D.T. Nguyen, M.C. Leopold, Langmuir **29**, 4574–4583 (2013)
114. J. Li, J. Yang, Z. Yang, Y. Li, S. Yu, Q. Xua, X. Hu, Anal. Methods **4**, 1725–1728 (2012)
115. B. Wang, J. Zhang, Y. Hu, S. Wang, R. Liu, C. He, X. Wang, H. Wang, Int. J. Electrochem. Sci. **8**, 7175–7186 (2013)
116. F. Lisdat, D. Schäfer, A. Kapp, Anal. Bioanal. Chem. **405**, 3739–3752 (2013)
117. Y. Liu, L. Zhu, J. Kong, P. Yang, B. Liu, Electrochem. Commun. **33**, 59–62 (2013)